Molecular Vision 2014; 20:1209-1224 <http://www.molvis.org/molvis/v20/1209>
Received 15 April 2014 | Accepted 9 September 2014 | Published 10 September 2014

S100A4 is upregulated in proliferative diabetic retinopathy and correlates with markers of angiogenesis and fibrogenesis

Ahmed M. Abu El-Asrar,[1] Mohd Imtiaz Nawaz,[1] Gert De Hertogh,[2] Kaiser Alam,[1] Mohammad Mairaj Siddiquei,[1] Kathleen Van den Eynde,[2] Ahmed Mousa,[1] Ghulam Mohammad,[1] Karel Geboes,[2] Ghislain Opdenakker[3]

[1]Department of Ophthalmology, College of Medicine, King Saud University, Riyadh, Saudi Arabia; [2]Laboratory of Histochemistry and Cytochemistry, University of Leuven, KU Leuven, Belgium; [3]Rega Institute for Medical Research, Department of Microbiology and Immunology, University of Leuven, KU Leuven, Belgium

Purpose: The calcium-binding protein S100A4 is implicated in cancer cell invasion and metastasis, the stimulation of angiogenesis, the progression of fibrosis, and inflammatory disorders. We investigated the expression of S100A4 and correlated it with clinical disease activity as well as with the levels of osteopontin (OPN), soluble syndecan-1, and vascular endothelial growth factor (VEGF) in proliferative diabetic retinopathy (PDR). To reinforce the findings at the functional level, we examined the expressions of S100A4 and OPN in the retinas of diabetic rats and in human retinal microvascular endothelial cells (HRMECs) following exposure to VEGF and the proinflammatory cytokine tumor necrosis factor-α (TNF-α).

Methods: Vitreous samples from 30 PDR and 30 nondiabetic patients, epiretinal membranes from 14 patients with PDR, the retinas of rats, and HRMECs were studied by enzyme-linked immunosorbent assay (ELISA), immunohistochemistry, western blot analysis, and co-immunoprecipitation.

Results: ELISA revealed a significant increase in the expressions of S100A4, OPN, soluble syndecan-1, and VEGF in vitreous samples from PDR patients compared to nondiabetic controls ($p = 0.001$; <0.001; <0.001; <0.001, respectively). Significant positive correlations were found between the levels of S100A4, OPN ($r = 0.52$, $p = <0.001$), soluble syndecan-1 ($r = 0.37$, $p = 0.012$), and VEGF ($r = 0.29$, $p = 0.044$). In epiretinal membranes, S100A4 was expressed in the vascular endothelial cells and stromal CD45-expressing leukocytes. A significant positive correlation was detected between the number of blood vessels expressing CD31 and the number of stromal cells expressing S100A4 ($r = 0.77$, $p = 0.001$). Western blot analysis revealed a significant increase in the expressions of S100A4 and both intact and cleaved OPN in vitreous samples from PDR patients compared to nondiabetic controls, as well as in the retinas of diabetic rats. Co-immunoprecipitation studies revealed a positive interaction between S100A4 and the receptor for advanced glycation end products (RAGE) in the retinas of diabetic rats. TNF-α—but not VEGF—induced the upregulations of S100A4 and both intact and cleaved OPN in HRMECs.

Conclusions: S100A4 represents a valuable vitreous marker molecule in the pathogenesis of PDR and might become a new target for the treatment of PDR.

Ischemia-induced angiogenesis and the expansion of the extracellular matrix (ECM) in association with the outgrowth of fibrovascular epiretinal membranes at the vitreoretinal interface are the pathological hallmarks of proliferative diabetic retinopathy (PDR). The formation of fibrovascular tissue often leads to severe visual loss due to a vitreous hemorrhage or a tractional retinal detachment (RD). Chronic, low-grade subclinical inflammation is responsible for many of the vascular lesions associated with PDR [1,2]. Persistent inflammation and neovascularization are critical for PDR progression. Recently, it was demonstrated that the processes of inflammation and angiogenesis are closely interconnected [3,4]. In several studies, the overexpressions of proinflammatory, proangiogenic, and profibrogenic growth factors and cytokines has been demonstrated in PDR [5-8].

Angiogenesis, the sprouting of new blood vessels from preexisting blood vessels, is a multistep process requiring the degradation of the basement membranes and the ECM, as well as of endothelial cell migration, proliferation, and tube formation [9]. Vascular endothelial growth factor (VEGF) is the main angiogenic factor in PDR that promotes neovascularization and vascular leakage [10]. The angiogenic switch involves, in part, the proteolytic degradation of basement membranes and ECM components by matrix metalloproteinases (MMPs). Recent reports demonstrated increased expressions of MMP-1, MMP-7, and MMP-9 in the vitreous fluids of patients with PDR [11]. Similar to other chronic forms of

Correspondence to: Ahmed M. Abu El-Asrar, Department of Ophthalmology, King Abdulaziz University Hospital, Old Airport Road, P.O. Box 245, Riyadh 11411, Saudi Arabia. Phone: 966-11-4775723; FAX: 966-11-4775724; email: abuasrar@KSU.edu.sa / abuelasrar@yahoo.com

inflammation, it is likely that other factors also function as regulators of inflammation, angiogenesis, and fibrosis in PDR, and the identification and characterization of these factors may result in the development of additional diagnostic markers and therapeutic agents. Several proinflammatory, proangiogenic, and profibrogenic factors may be linked to the development and progression of PDR, including S100A4, osteopontin (OPN), and soluble syndecan-1.

S100A4, also known as metastasis-associated protein mts 1, is a calcium-binding protein associated with the invasion and metastasis of cancer cells, and it has been reported to be frequently overexpressed in metastatic tumors and in several types of cancers [12-14]. S100A4 is a well-established marker of tumor progression, invasion, and metastasis formation, as well as of prognosis in various human cancers [14,15]. Recently, S100A4 has been implicated in the progression of fibrosis in various organs [16-21] and has been linked to inflammatory disorders, such as rheumatoid arthritis [22-24]. The common feature of all these pathological conditions is that both inflammation and fibrosis are involved. These processes also depend on tissue remodeling and cell motility [25]. S100A4 is localized in the nucleus, cytoplasm, and extracellular space and it possesses a wide range of biologic functions, such as the regulations of cell motility, migration, proliferation, invasion, and survival, as well as the stimulation of angiogenesis and the remodeling of the ECM [14,25,26]. In the extracellular space, S100A4 has been reported to interact with the receptor for advanced glycation end products (RAGE). Intracellularly, it activates transcription factors, such as nuclear factor kappa B (NF-κB) [13,14,25]. It has been reported that the S100A4 gene controls the invasiveness, growth, angiogenesis, and metastasis of several types of cancers through the transcriptional activation of MMP-9 [12,13,27]. In addition, it was demonstrated that the S100A4-induced angiogenesis of cancer cells was, in part, through the VEGF pathway [27], that the S100A4-positive stromal cells support metastatic colonization via production of VEGF, and that S100A4-positive stromal cell-derived VEGF appears important to the establishment of an angiogenic microenvironment at the site of metastasis [28].

OPN is a phosphorylated acidic arginine-glycine-aspartate (RGD)-containing glycoprotein that exists both as an immobilized ECM component and as a soluble multifunctional proinflammatory cytokine, which play important roles in promoting inflammation [29,30], tissue remodeling, fibrosis [29,31-34], and angiogenesis [35-38]. Many of these effects are mediated by the binding of OPN to CD44 receptors and the surface integrin receptor αvβ3 [35,36,39]. Several studies reported that the proinflammatory cytokine OPN is a hyperglycemia-induced cytokine and that OPN plays a role in the development of diabetic vascular inflammatory complications [29,40-42]. Recent reports demonstrated that OPN increases VEGF expressions in several cell types [35,43]. A recent study demonstrated that S100A4 induces NF-κB-dependent expressions and secretions of OPN in osteosarcoma cell lines [44]. These findings suggest that OPN may be a molecular mechanism related to S100A4 signaling.

Syndecans are a small family of type 1 transmembrane heparan sulfate-bearing proteoglycans. The four mammalian members—syndecan-1 to syndecan-4—all comprise an ectodomain, a single transmembrane domain, and a short cytoplasmic domain [45]. The ectodomains of the syndecans are constitutively shed to a small degree under physiologic conditions, but this may be dramatically increased in response to stimuli [45]. Such ectodomain shedding generates soluble ectodomains that can function as paracrine or autocrine effectors. Evidence indicates that several MMPs, including MMP-2, MMP-3, MMP-7, and MMP-9, cleave the ectodomains of syndecan-1, thereby releasing it from the cell surface as an intact extracellular ectodomain bearing heparan sulfate chains [46]. Soluble (shed) syndecan-1 can actively promote inflammation, angiogenesis, tumor cell growth, and metastasis [46].

Given the key roles of S100A4, OPN, and soluble syndecan-1 in inflammation, angiogenesis, and fibrosis, we hypothesized that these molecules may be involved in the pathogenesis of PDR. To test this hypothesis, we investigated the expressions of S100A4, OPN, and soluble syndecan-1 in the vitreous fluids and epiretinal membranes of patients with PDR, and their levels were correlated with the levels of the angiogenic factor VEGF. In addition to corroborating a functional link between these molecules in diabetes, we investigated the expressions of S100A4 and OPN in the retinas of diabetic rats and in human retinal microvascular endothelial cells (HRMECs) following exposure to VEGF and the proinflammatory cytokine tumor necrosis factor-α (TNF-α).

METHODS

Vitreous samples and epiretinal membrane specimens: Undiluted vitreous fluid samples (0.3–0.6 ml) were obtained from 30 patients with PDR during pars plana vitrectomy. The indications for vitrectomy were tractional RD or a nonclearing vitreous hemorrhage. The control group consisted of 30 patients who had undergone vitrectomy for the treatment of rhegmatogenous RD with no proliferative vitreoretinopathy. Controls were free from systemic disease. Vitreous samples were collected undiluted by manual suction into a syringe through the aspiration line of the vitrectomy

unit before opening the infusion line. The samples were centrifuged (700 ×g for 10 min, 4 °C), and the supernatants were aliquoted and frozen at −80 °C until assay. Epiretinal fibrovascular membranes were obtained from 14 patients with PDR during pars plana vitrectomy for the repair of tractional RD. Membranes were fixed for 2 h in 10% formalin solution and embedded in paraffin. The severity of retinal neovascular activity was graded clinically at the time of vitrectomy using previously published criteria [47]. Neovascularization was considered active if there were visibly new perfused vessels on the retina or optic disc, as well as if it was present within the tractional epiretinal membranes. Neovascularization was considered inactive (involuted) if only nonvascularized white fibrotic epiretinal membranes were present.

The study was conducted according to the tenets of the Declaration of Helsinki. All the patients were candidates for vitrectomy as a surgical procedure. All patients provided preoperative informed written consent and approved the use of the excised epiretinal membranes and vitreous fluids for further analysis and clinical research. The study design and the protocol were approved by the Research Centre and Institutional Review Board of the College of Medicine, King Saud University.

Rat streptozotocin-induced diabetes model: All procedures with animals were performed in accordance with the ARVO statement on the use of animals in ophthalmic and vision research and were approved by the Institutional Animal Care and Use Committee of the College of Pharmacy, King Saud University. Adult male Sprague-Dawley rats, at 8–9 weeks of age and weighing in the range of 220–250 g, were overnight fasted and injected with streptozotocin (STZ; 65 mg/kg in 50 mM sodium citrate buffer, pH 4.5; Sigma, St. Louis, MO) intraperitoneally. Equal volumes of citrate buffer were injected into the control non-diabetic animals. Measurements of blood glucose concentrations and body weight were taken 3 days after injection of STZ. Diabetes was confirmed by assaying the glucose concentration in blood taken from the tail vein. Rats with glucose levels greater than 250 mg/dl were categorized as diabetic. After 4 weeks of diabetes, animals were anesthetized by intraperitoneal injection of an overdose of chloral hydrate and sacrificed by decapitation. Retinas were dissected, flash frozen, and stored at −70 °C until use. Similarly, retinas were obtained from age-matched nondiabetic control rats.

Cell culture: Primary HRMECs were purchased from Cell Systems Corporation (Kirkland, WA), maintained in complete serum-free media (Cat. No. SF-4Z0–500, Cell System Corporation), and supplemented with recombinant RocketFuel (Cat No. SF-4ZO-500, Cell System Corporation), CultureBoost (Cat. No. 4CB-500, Cell System Corporation), and antibiotics (Cat. No. 4ZO-643, Cell System Corporation) at 37 °C in a humidified atmosphere with 5% CO_2. We used HRMECs up to passage 8 for all the experiments. When the HRMECs became about 80% confluent, cells were starved in a medium without growth factors (RocketFuel and CultureBoost) overnight to eliminate any residual effects of the growth factors. Following starvation, HRMECs were either left untreated or treated with 30 ng/ml of TNF-α (Cat. No. 210-A-050, R&D Systems, Minneapolis, MN) or 10 ng/ml of VEGF (Cat. No. 298-VS025, R&D Systems). The medium was replaced along with the respective cytokines every 48 h. Cells were harvested after 6 days for an analysis of the expression levels of the OPN and S100A4 proteins.

Enzyme-linked immunosorbent assay: An enzyme-linked immunosorbent assay (ELISA) kit for human S100A4 (Human CircuLex S100A4, Cat No: CY-8086) was purchased from CycLex Co., Ltd., Ina, Japan. ELISA kits for human VEGF (Cat No: SVE00), human syndecan-1 (Cat No: DY2780), and human OPN (Cat No: DY1433) were purchased from R&D Systems. The minimum detection limit for the S100A4 and VEGF ELISA kits were 0.282 ng/mL and 9 pg/ml, respectively. The ELISA plate readings were done using a Stat Fax-4200 microplate reader from Awareness Technology, Inc., Palm City, FL.

Measurements of S100A4, OPN, soluble syndecan-1, and VEGF: The quantification of human S100A4, OPN, soluble syndecan-1, and VEGF in vitreous fluids was determined using ELISA kits according to the manufacturer's instructions. For each ELISA kit, the undiluted standard was served as the highest standard and calibrator diluents were served as the zero standard. Depending on the detection range for each ELISA kit, vitreous fluid samples were adequately diluted with calibrator diluents supplied with each ELISA kit.

For the measurements of S100A4 and OPN, respectively, 100 µl of 4-fold and 1,000-fold diluted vitreous samples were analyzed with the respective ELISA assays. For the measurement of soluble syndecan-1 and VEGF, 100 µl of undiluted vitreous samples were used. As instructed in the kit manual, samples were incubated into each well of the ELISA plates. Antibodies against S100A4, OPN, soluble syndecan-1, and VEGF conjugated to horseradish peroxidase (HRP) were added to each well of the ELISA plates. After incubation, a substrate mix solution was added for color development. The reaction was stopped by the addition of 2N sulfuric acid (R&D Systems), and the optical density was read at 450 nm in a microplate reader. Each assay was performed in duplicate. Using the 4-parameter fit logistic (4-PL) curve equation, the actual concentration of each sample was calculated. For the

diluted vitreous fluids, the correction read from the standard curve obtained using 4-PL was multiplied by the dilution factor to calculate the actual reading for each sample.

Western blot analysis: Retinas from diabetic and control rats were homogenized in western blot lysis buffer (30 mM Tris-HCl; pH 7.5, 5 mM EDTA, 1% Triton X-100, 250 mM sucrose, 1 mM Sodium vanadate, and protease inhibitor cocktail). The protease inhibitor used was "Complete without EDTA" (Roche, Mannheim, Germany). The homogenates were centrifuged at 14,000 ×*g* for 15 min at 4 °C and the supernatants were used for protein estimation and further analysis. HRMECs—treated either with TNF-α or VEGF for 6 days or untreated—were harvested and lysed with RIPA buffer (50 mM Tris/HCl [pH 7.5], 150 mM NaCl, 1% (v/v) Nonidet P40 (NP-40), 0.5% Sodium deoxycholate, 0.1% SDS, and protease inhibitor). Whole-cell extracts from different groups were centrifuged at 14,000×*g* for 15 min at 4 °C. The supernatants were collected and protein concentrations were measured using a DC protein assay kit (Bio-Rad Laboratories, Hercules, CA). For a determination of the expressions of OPN and S100A4, equal amounts of protein (45–60 ug) were subjected to SDS-polyacrylamide gel electrophoresis (SDS-PAGE) with 8–12% gel. To determine the expression levels of S100A4 and OPN in the vitreous samples, equal volumes of vitreous samples were boiled in 2X Laemmli's sample buffer (1:1, v/v) under reducing conditions for 10 min. Equal volumes of lysis solution (15 µl) were loaded and separated by 10–12% SDS-PAGE. Separated proteins were transferred onto nitrocellulose membranes. Nonspecific binding sites were blocked for 1 h at room temperature in a blocking buffer (5% non-fat dry milk in PBS and 0.02% Tween-20). Blots were then incubated at 4 °C overnight using the following primary antibodies: S100A4 (1:500; sc-292281; Santa Cruz Biotechnology Inc., Santa Cruz, CA) and an anti-OPN antibody (1:1000; ab-8448; Abcam, Cambridge, UK). Three PBS-T washings (5 min each) were performed before respective secondary antibody treatment at room temperature for 1 h. Finally, immunodetection was performed with the chemiluminescense western blotting luminol reagent (sc-2048; Santa Cruz Biotechnology Inc.). Membranes were stripped and reprobed with β-actin (1:2000; sc-47778; Santa Cruz Biotechnology Inc.) to evaluate sample processing and the lane-loading controls. Bands were visualized with the use of a high-performance chemiluminescence machine (G: Box Chemi-XX8 from Syngene, Synoptic Ltd. Cambridge, UK), and the intensities were quantified using the GeneTools software (Syngene by Synoptic Ltd.). To ascertain a similar protein loading for a western blot analysis of vitreous fluid samples, Coomassie brilliant blue staining for proteins was used. Equal volumes of vitreous fluid samples (10 µl) were separated by SDS-PAGE in 10% gel, and all proteins in the resultant gel were visualized after staining.

Co-immunoprecipitation: Retina tissue was homogenized in 30 mM of Tris-HCl lysis buffer (pH 7.5) containing 10 mM EGTA, 5 mM EDTA, 1% Triton X-100, 250 mM sucrose, 1 mM NaF, 1 mM phenylmethylsulfonyl fluoride, 1 mM Na_3VO_4, and protease inhibitor. Protein (150µg) was incubated overnight at 4 °C with 2 µg of the anti-S100A4 antibody and the normal rabbit IgG control antibody (Cat. No. AB-105-C, R&D Systems). Prewashed protein A/G plus agarose beads (20 µl of bead slurry; Santa Cruz Biotechnology, Inc.) were then added to the mixture and rolled for 1 h at 4 °C. After centrifugation, immunoprecipitates were washed 4X with lysis buffer. After the last wash, the resultant pellets were resuspended in 20 µl of 2X Laemmli's sample buffer and then denatured for 5 min at 95 °C, separated by gel electrophoresis, and transferred to polyvinyl difluoride membranes. This was followed by immunoblotting with an anti-RAGE antibody (1:500; sc-5563; Santa Cruz Biotechnology Inc.) and detection with chemiluminescence plus a Luminol HRP substrate. To evaluate the lane-loading control, the blots were stripped and the S100A4 protein was detected with the anti-S100A4 antibody.

Immunohistochemical staining: For CD31, antigen retrieval was performed by boiling the sections in a citrate-based buffer (pH 5.9–6.1; BOND Epitope Retrieval Solution 1; Leica) for 10 min. For S100A4 and CD45 detection, antigen retrieval was performed by boiling the sections in a Tris/EDTA buffer (pH 9; BOND Epitope Retrieval Solution 2; Leica) for 20 min. Subsequently, the sections were incubated for 60 min with mouse monoclonal anti-CD31 (ready-to-use; clone JC70A; Dako, Glostrup, Denmark), mouse monoclonal anti-CD45 (ready-to-use; clones 2B11+PD7/26; Dako), and rabbit polyclonal anti-S100A4 (1:50; ab-113527; Abcam). Optimal working concentrations and incubation times for the antibodies were determined earlier in pilot experiments using sections from patients with glioblastoma and Crohn's disease. The sections were then incubated for 20 min with a post primary IgG linker followed by an alkaline phosphatase conjugated polymer. The reaction product was visualized by incubation for 15 min with the Fast Red chromogen, resulting in bright red immunoreactive sites. The slides were then faintly counterstained with Mayer's hematoxylin (BOND Polymer Refine Red Detection Kit; Leica).

To identify the phenotypes of cells expressing S100A4, sequential double immunohistochemistry was performed. The sections were incubated with the first primary antibody (anti-CD45) and subsequently treated with a peroxidase conjugated secondary antibody. The sections were visualized

with 3,3′-diaminobenzidine tetrahydrochloride. Incubation of the second primary antibody (anti-S100A4) was followed by treatment with an alkaline phosphatase conjugated secondary antibody. The sections were visualized with the Fast Red chromogen. No counterstain was applied.

Omission or substitution of the primary antibody with an irrelevant antibody from the same species (rabbit monoclonal anti-human estrogen receptor α; ready-to-use; clone EPI, Dako) and staining with a chromogen alone were used as negative controls. Sections from patients with glioblastoma and Crohn's disease were used as positive controls for the immunohistochemical staining methods.

Quantitation: Immunoreactive blood vessels and cells were counted in five representative fields using an eyepiece-calibrated grid in combination with a 40X objective. These representative fields were selected based on the presence of immunoreactive blood vessels and cells. With this magnification and calibration, immunoreactive blood vessels and cells present in an area of 0.33×0.22 mm^2 were counted.

Statistical analysis: Data are presented as the mean ± standard deviation. The non-parametric Mann–Whitney test was used to compare the means from two independent groups. A chi-square test was used to compare proportions when analyzing data for two categorical variables. Pearson correlation coefficients were computed to investigate correlations between variables and a p value less than 0.05 indicated statistical significance. SPSS version 20.0 for Windows (IBM Inc., Chicago, IL) was used for statistical analysis.

RESULTS

ELISA levels of S100A4, OPN, soluble syndecan-1, and VEGF in vitreous samples: With the use of ELISA, we demonstrated that S100A4, OPN, and soluble syndecan-1 were detected in all vitreous samples from patients with PDR, as well as from control patients without diabetes (Figure 1). The mean levels of S100A4, OPN, and soluble syndecan-1 in vitreous samples from PDR patients were significantly higher than the levels in nondiabetic patients ($p = 0.001$; $p<0.001$; $p<0.001$, respectively; Mann–Whitney test; Table 1). A comparison of the mean levels of S100A4 between active and inactive PDR patients indicated that the mean S100A4 level was significantly higher in patients with active PDR (n = 16; 24.6 ± 30.7 ng/ml) than in patients with inactive PDR (n = 14; 11.5 ± 25.5 ng/ml; $p = 0.045$, Mann–Whitney test).

We used the analysis of VEGF levels as an internal control. In line with previous findings [11], VEGF was detected in 13 of 28 (46.4%) vitreous samples from nondiabetic control patients, as well as in 23 of 27 (82.1%) samples from patients with PDR ($p = 0.014$; chi-square test; Figure 1). The mean VEGF level in vitreous samples from PDR patients (845.3 ± 975.1 pg/ml) was significantly higher than the mean level in nondiabetic control patients (54.2 ± 117.5 pg/ml; $p<0.001$; Mann–Whitney test; Table 1).

Correlations: Significant positive correlations were found between the vitreous fluid levels of S100A4, as well as of OPN ($r = 0.52$; $p<0.001$), soluble syndecan-1 ($r = 0.37$; $p = 0.012$), and VEGF ($r = 0.29$; $p = 0.044$). There were significant correlations between the vitreous fluid levels of OPN, as well as of soluble syndecan-1 ($r = 0.41$; $p = 0.003$) and VEGF ($r = 0.31$; $p = 0.026$; Figure 2). Although these correlations were weak to moderate, they were statistically significant.

Western blot analysis of vitreous samples: Protein contents in equal volumes of the vitreous fluid samples were confirmed by Coomassie brilliant blue staining (Figure 3A). The most abundant protein band in all the samples was albumin, followed by collagen type II. The presence of albumin is most likely the result of a breakdown of the blood retinal barrier. The most abundant structural protein from the vitreous is type II collagen, accounting for approximately 80% of vitreous collagen [48-50]. We used collagen type II as a vitreous control protein. To ascertain that similar vitreous protein amounts were contained in equal vitreous volumes of the diabetes and control samples, we compared the collagen type II contents. A densitometric analysis of the protein bands demonstrated that the amount of collagen type II did not differ significantly among the vitreous samples in patients with PDR compared to the control patients (Figure 3 A). A western blot analysis was also used to quantify the expression levels of S100A4 and OPN in vitreous samples from patients with PDR (n = 16) and control patients without diabetes (n = 15). A densitometric analysis of the bands demonstrated a significant increase in S100A4 ($p = 0.012$; Mann–Whitney test) in vitreous samples from PDR patients compared to control patients (Figure 3B). OPN protein migrated as two protein bands on SDS-PAGE when immunoblotted and analyzed with a specific antibody. The upper band corresponded to the intact protein, whereas the lower protein band corresponded to cleaved OPN (around 45 kDa). A densitometric analysis of the bands demonstrated a significant increase in the full-length protein ($p = 0.043$; Mann–Whitney test) and the 45-kDa fragment ($p = 0.032$; Mann–Whitney test) expressions in vitreous samples from PDR patients compared to control patients (Figure 3B).

Immunohistochemical analysis of epiretinal membranes: To identify the cell source of vitreous fluid S100A4, epiretinal membranes from patients with PDR were studied by immunohistochemical analysis. No staining was observed in the negative control slides (Figure 4A). The level of vascularization

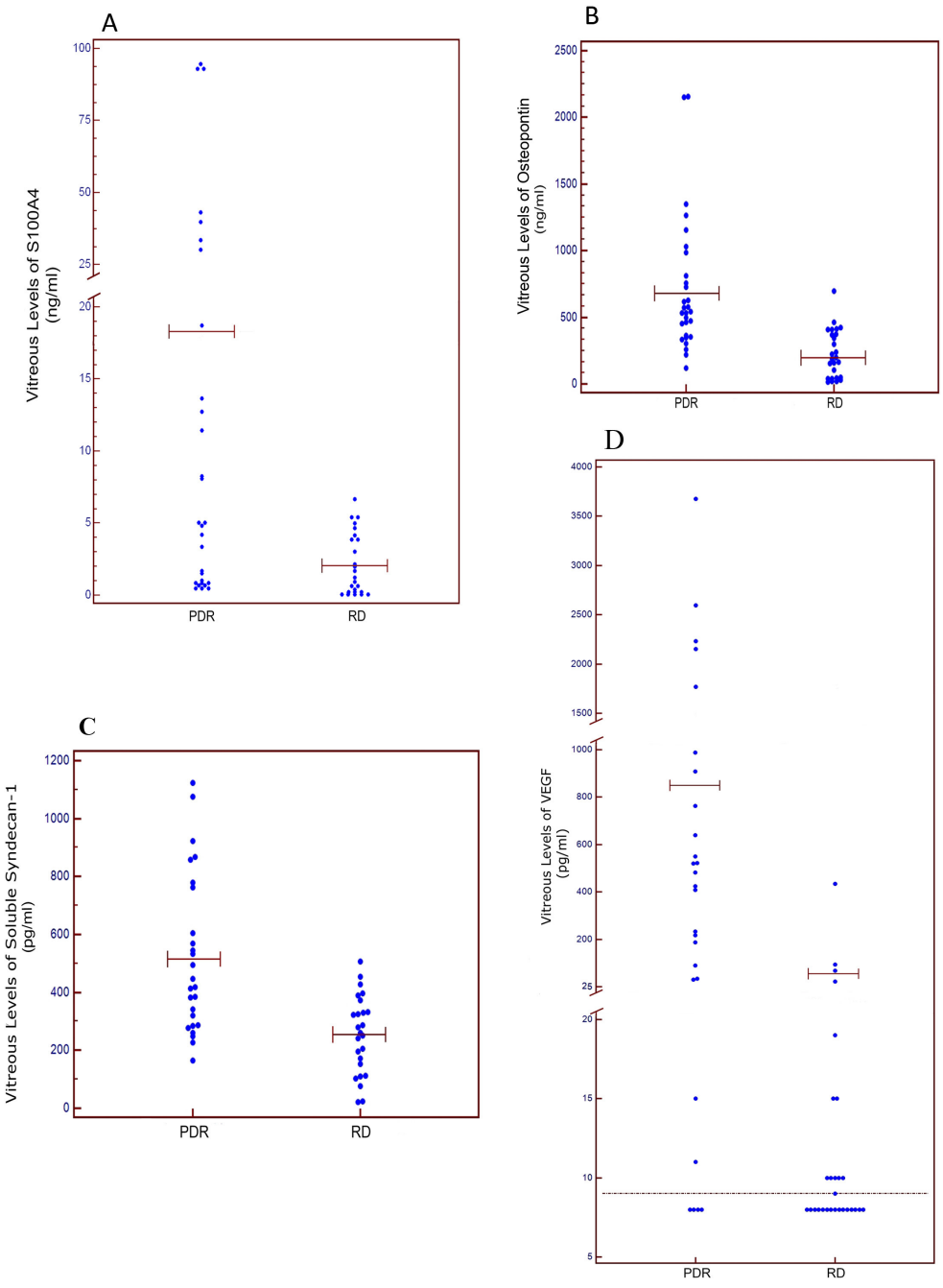

Figure 1. Detectable levels of S100A4 (panel **A**), osteopontin (OPN; panel **B**), soluble syndecan-1 (panel **C**), and vascular endothelial growth factor (VEGF; panel **D**) in vitreous samples from eyes with proliferative diabetic retinopathy (PDR) and rhegmatogenous retinal detachment (RD). The dashed line represents the detection limit (9 pg/ml) of the assay for VEGF (panel **D**). The mean levels are indicated by horizontal solid lines.

and proliferative activity in epiretinal membranes were determined by immunodetection of the endothelial cell marker CD31. All membranes showed blood vessels that were positive for the endothelial cell marker CD31 (Figure 4B), with a mean of 43.4 ± 45.4 (range, 12–125) per studied field. Strong immunoreactivity for S100A4 was present in all membranes and was noted in stromal cells (Figure 4C) and vascular endothelial cells (Figure 4D). The majority of S100A4-positive stromal cells were monocytes or macrophages. In serial sections, the distributions and morphologies of stromal cells expressing S100A4 were similar to those of cells expressing the leukocyte common antigen CD45 (Figure 4E). Double staining confirmed that stromal cells expressing S100A4 co-expressed CD45 (Figure 4F). The number of blood vessels that were immunoreactive for S100A4 ranged from one to 30, with a mean of 9.9 ± 9.3 per studied field. The number of immunoreactive stromal cells ranged from 10 to 195, with a mean of 74.9 ± 63.7 per analyzed microscopic field.

Table 1. Comparison of mean levels in proliferative diabetic retinopathy (PDR) and rhegmatogenous retinal detachment (RD) patients.

Disease group	S100A4 (ng/ml)	Osteopontin (ng/ml)	Soluble Syndecan-1 (pg/ml)	VEGF (pg/ml)
PDR	18.3±28.6	709.7±504.4	522.8±272.9	845.3±975.1
RD	2.1±2.1	227.1±180.5	254.2±134.7	54.2±117.5
P value (Mann–Whitney test)	0.001*	<0.001*	<0.001*	<0.001*

*Statistically significant at 5% level of significance. VEGF=vascular endothelial growth factor

The mean number of blood vessels expressing CD31 was significantly higher in membranes from patients with active PDR (n = 5; 98.4 ± 25.6) than in membranes from patients with inactive PDR (n = 9; 12.9 ± 8.3; p = 0.001; Mann–Whitney test). The difference between the mean number of blood vessels expressing S100A4 in membranes from patients with active PDR (14 ± 7.2) and in membranes from patients with inactive PDR (7.6 ± 9.9) was not significant (p = 0.112; Mann–Whitney test). The mean number of stromal cells immunoreactive for S100A4 was significantly higher in membranes from patients with active PDR (139 ± 42.6) than in membranes from patients with inactive PDR (39.2 ± 41.2; p = 0.004; Mann–Whitney test). A significant positive correlation was detected between the number of blood vessels expressing CD31 and the number of stromal cells expressing S100A4 (r = 0.77, p = 0.001). On the other hand, the correlation between the number of blood vessels expressing CD31 and the number of blood vessels expressing S100A4 was not significant (r = 0.47, p = 0.093).

Severity of hyperglycemia and effect of diabetes on retinal expressions of S100A4 and OPN in experimental rats: To validate our observations and to obtain a better view of the studied molecules in the pathogenesis of diabetic retinopathy, we used a rat animal model. After induction of diabetes with a single high-dose of streptozotocin, the body weights of the diabetic rats were significantly lower and their blood glucose values were more than 4-fold higher when compared with age-matched normal control rats (168 ± 25 versus 293 ± 22 g and 478 ± 29 versus 111 ± 11 mg/dl, respectively). We quantified the expressions of S100A4 and OPN in rat retinas by western blot analysis. A densitometric analysis of the bands revealed a significant increase in S100A4 in diabetic retinas compared to nondiabetic controls (p = 0.027; Mann–Whitney test; Figure 5). OPN protein migrated as two protein bands on SDS-PAGE when immunodetected with a specific antibody. The upper band corresponded to the intact protein, whereas the lower protein band corresponded to cleaved rat OPN (32 kDa). A densitometric analysis of the bands revealed a significant increase in both intact OPN (p = 0.027; Mann–Whitney test) and cleaved OPN (p = 0.001; Mann–Whitney test) in diabetic retinas compared to nondiabetic controls (Figure 5).

Interaction between S100A4 and RAGE: Co-immunoprecipitation studies were performed on retina extracts of nondiabetic control and diabetic rats. In the diabetic retinas, there was an increased interaction between S100A4 and RAGE (p = 0.047; Mann–Whitney test; Figure 6).

TNF-α—but not VEGF—induced upregulation of S100A4 and OPN in HRMECs: In view of the described correlations and the fact that we previously found an increase in the expression of TNF-α in epiretinal membranes from patients with PDR [51], we also tried to validate at the endothelial cell level our preclinical and clinical observations with the use of cultured HRMECs. After 6 days of cell culture, western blot analysis revealed significant upregulations of S100A4 (p = 0.028; Mann–Whitney test) and both intact (p = 0.007; Mann–Whitney test) and cleaved (32 kDa; p<0.001; Mann–Whitney test) OPN in response to TNF-α treatment (Figure 7). In contrast, VEGF treatment did not affect the expressions of S100A4 and OPN (data not shown).

DISCUSSION

In the present study, we showed for the first time that S100A4 was significantly upregulated in vitreous fluids from patients with PDR and in the retinas of diabetic rats, as well as that the proinflammatory cytokine TNF-α—but not VEGF—induced the upregulation of S100A4 in HRMECs. Our subgroup analysis showed that the S100A4 levels in vitreous samples from active PDR cases were higher than in quiescent cases. Using immunohistochemistry, we demonstrated that the S100A4 protein was specifically localized in vascular endothelial cells and leukocytes expressing the leukocyte common antigen CD45 in the epiretinal membranes from patients with

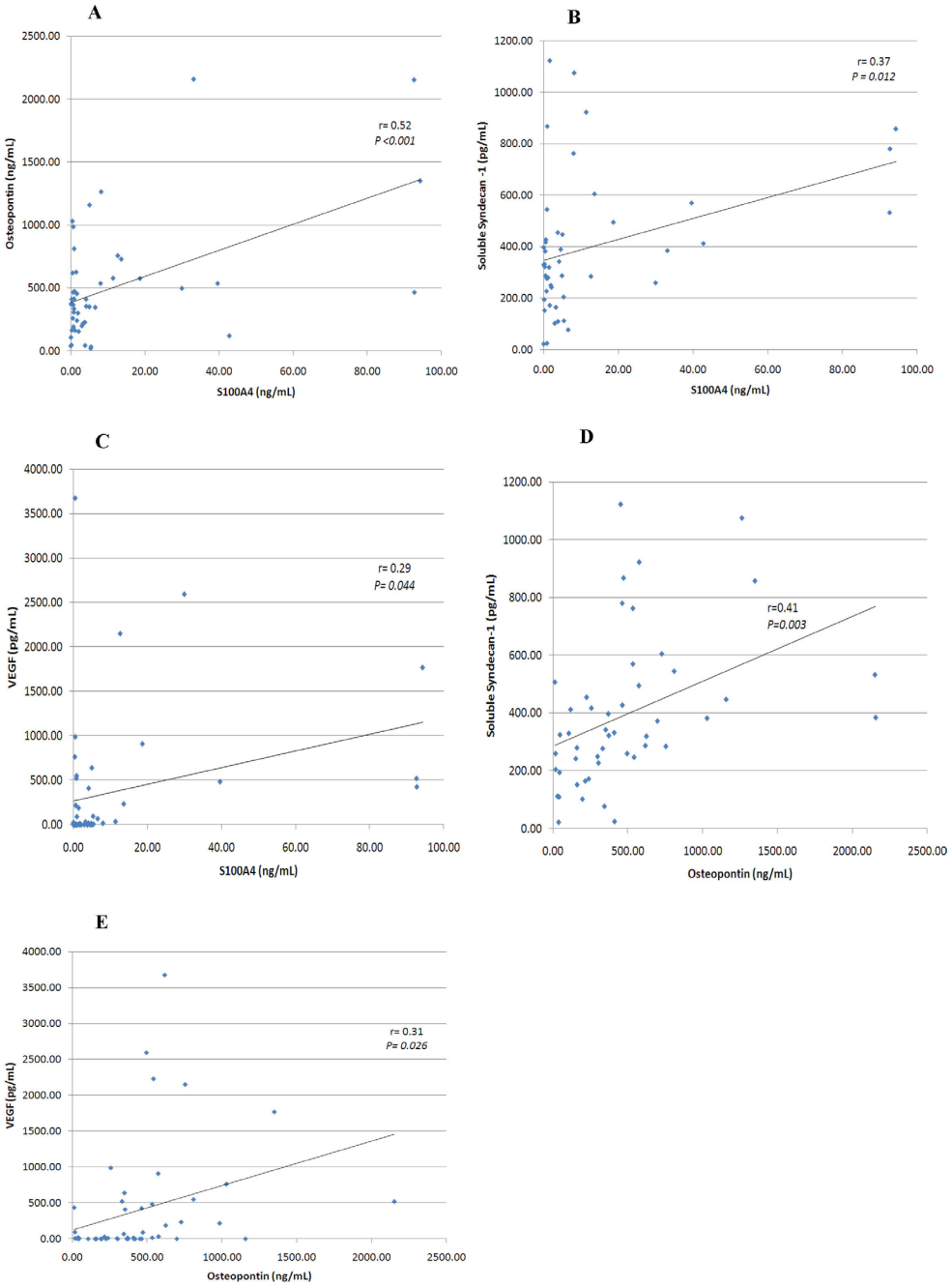

Figure 2. Significant positive correlations between the vitreous fluid levels of S100A4 and the levels of OPN (panel **A**), soluble syndecan-1 (panel **B**), and VEGF (panel **C**), as well as between the vitreous fluid levels of OPN and the levels of soluble syndecan-1 (panel **D**) and VEGF (panel **E**).

PDR, and there was a significant positive correlation between the level of vascularization in PDR epiretinal membranes and the number of stromal cells expressing S100A4. Moreover, the expression of S100A4 in membranes from patients with active neovascularization was significantly higher than in membranes from patients with inactive PDR. Similarly, previous studies demonstrated that vessel density and S100A4 were positively correlated in the primary tumors of patients with breast cancer [15]. The immunoreactivity for S100A4 in leukocytes and endothelial cells in the present study is compatible with previously published data [15,21-23,52]. Together, these findings suggest that S100A4 is a useful marker of the progression of PDR.

Recently, S100A4 has been identified as a potent stimulator of angiogenesis. The extracellular S100A4 protein is capable of enhancing endothelial cell motility in vitro and it stimulates corneal neovascularization in vivo [53]. It was demonstrated that S100A4 synergizes with VEGF via the

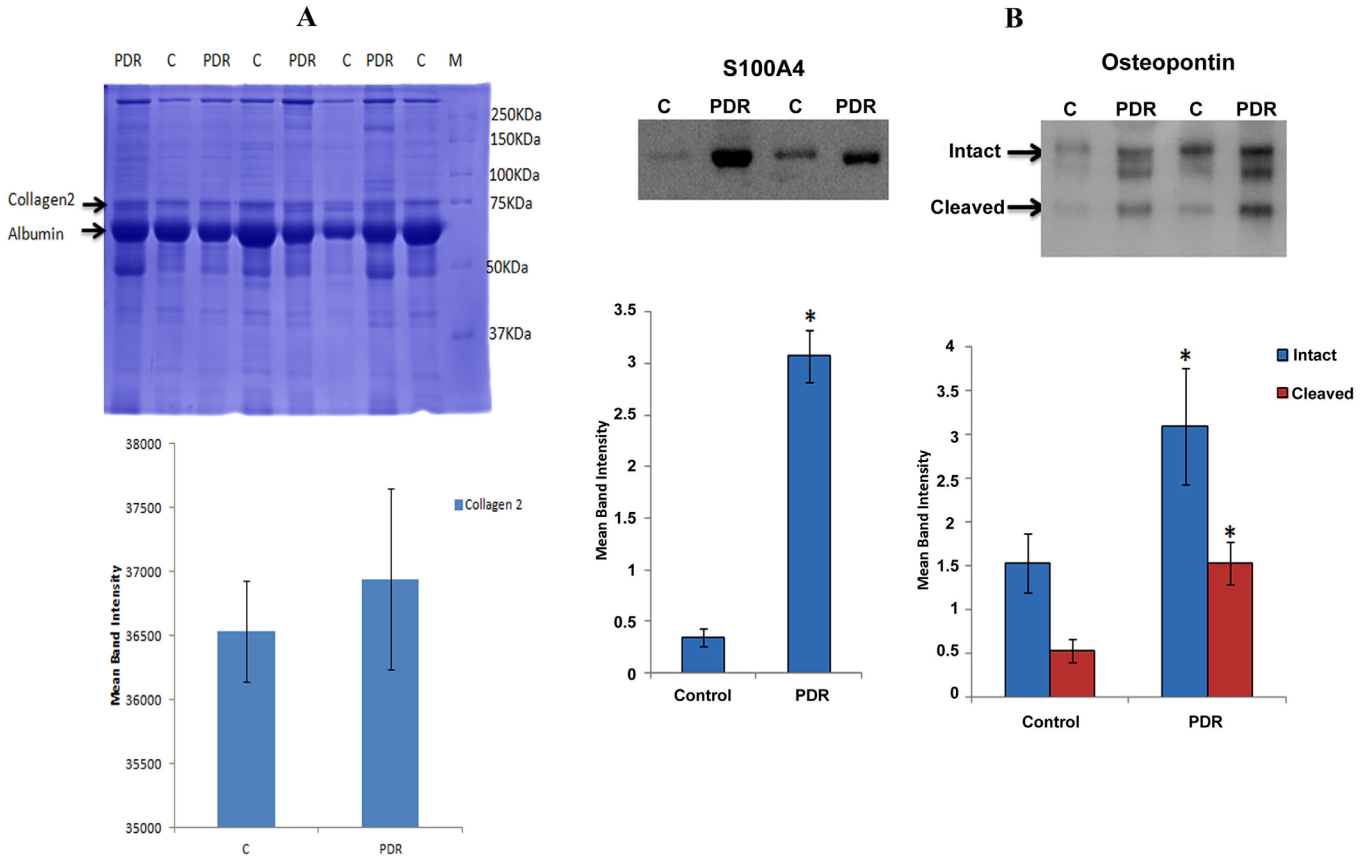

Figure 3. Vitreous fluid samples obtained from PDR and control patients (C) were separated by 10% SDS-PAGE, and proteins in the resultant gel were visualized by Coomassie brilliant blue staining (panel **A**). The top arrow represents collagen type II (molecular weight approximately 72 kDa) and the lower arrow represents albumin (molecular weight approximately 66 kDa). The intensity of the protein staining of collagen type II was quantitated by densitometry of eight PDR and eight control samples. The resultant data are presented in the histograms as mean ± standard deviation and they were comparable for both groups. The levels of S100A4 and OPN in vitreous samples from patients with PDR and from control patients without diabetes (**C**) were determined by western blot analysis (panel **B**). A representative set of samples is shown. The expressions of S100A4 and both intact and cleaved OPN are significantly increased in vitreous samples from PDR patients compared to control patients without diabetes. *The difference between the two means was statistically significant at the 5% level.

RAGE in promoting endothelial cell migration [54]. An over-expression of S100A4 in thyroid cancer cells led to increased tumor angiogenesis and increased the expressions and activities of VEGF and MMP-9 [27]. Ochiya et al. [55] showed the importance of the endothelial S100A4 expression in tumor angiogenesis. In addition, S100A4-expressing stromal cells supported metastatic colonization via the production of VEGF [28]. A blockade of extracellular S100A4 with a specific monoclonal antibody reduces endothelial cell migration induced by a combination of S100A4 and VEGF, and it reduces tumor angiogenesis and growth in vivo, blocks the production of active forms of MMP-9 induced by S100A4, and blocks the interaction between S100A4 and the RAGE [54]. In the current study, we found a significant correlation between the vitreous levels of S100A4 and those of the angiogenic biomarker VEGF. This finding is consistent with previous studies that reported significant positive correlations between S100A4 and VEGF expressions in patients with several types of cancers [56,57].

Recent studies have linked S100A4 to several diseases besides cancer, including inflammatory disorders and the progression of fibrosis in various organs. These processes greatly depend on tissue remodeling and cell motility [25]. S100A4-positive cells are increased in experimental models of renal fibrosis [17,18], cardiac fibrosis [16,19,20], and liver disease [21]. In rheumatoid arthritis, the S100A4 expression is upregulated in the synovial tissue accompanied by high synovial fluid and the plasma concentrations of S100A4 [22,23]. In addition, the plasma levels of S100A4 are significantly correlated with disease activity [24]. In the present study, the co-immunoprecipitation results showed that diabetes increased the interaction between S100A4 and the RAGE in

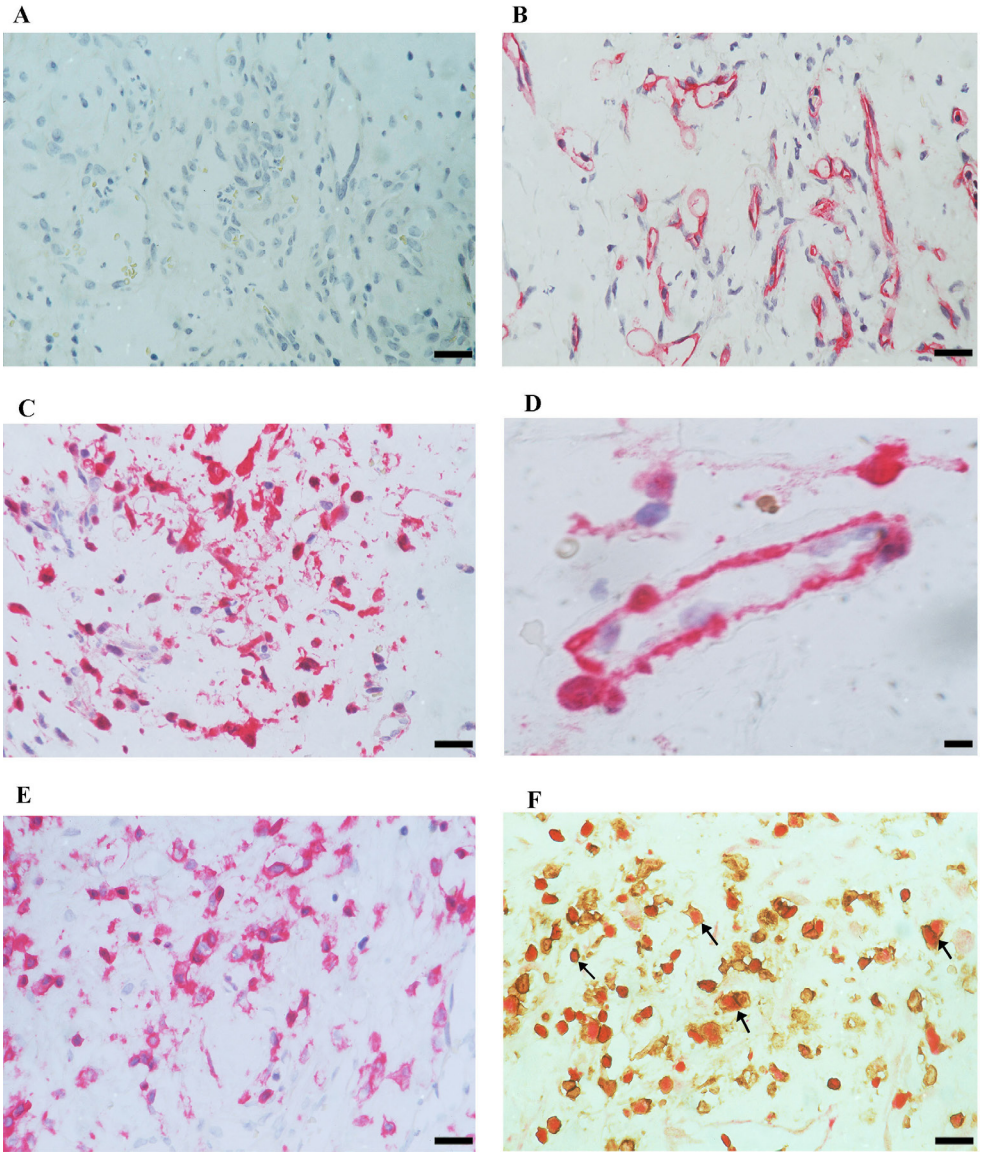

Figure 4. PDR epiretinal membrane immunostainings. A negative control slide that was treated with an irrelevant antibody showing no labeling (panel **A**; scale bar, 10 µm). Immunohistochemical staining for CD31 showing blood vessels positive for CD31 (panel **B**; scale bar, 10 µm). Immunohistochemical staining for S100A4 showing immunoreactivity in stromal cells (panel **C**; scale bar, 10 µm) and in the vascular endothelium (panel **D**; scale bar, 8 µm). Immunohistochemical staining for CD45 showing stromal cells positive for CD45 (panel **E**; scale bar, 10 µm). Double immunohistochemistry for CD45 (brown) and S100A4 (red) showing stromal cells co-expressing CD45 and S100A4 (arrows; panel **F**; scale bar, 10 µm).

the retina. These results suggest that in the diabetic retina, S100A4 mediates the proinflammatory, proangiogenic, and profibrogenic pathways through the RAGE. A recent study demonstrated the RAGE-dependent increase in the migratory and invasive capabilities of colorectal cancer cells via binding to extracellular S100A4 [58]. In previous studies, we demonstrated a significant upregulation of RAGE in the retinas of diabetic rats [59], as well as that RAGE was expressed in PDR epiretinal membranes and was localized in vascular endothelial and stromal cells [60].

In this study, we report that OPN levels were significantly upregulated in the vitreous fluids of patients with PDR. These results are consistent with our previous reports [6,60]. In addition, we demonstrated the upregulated expressions of both intact and cleaved OPN in the retinas of diabetic rats. Our western blot analysis demonstrated the presence of intact and cleaved (molecular weight of around 45 kDa) OPNs in the vitreous fluids of PDR patients. OPN has been recognized as a substrate for proteolytic cleavage by members of the MMP family. Of interest is the fact that rather than degrade OPN, these proteases enhance the ability of OPN to promote cell adhesion and migration [61], metastatic tumor invasion [62], and macrophage infiltration [60]. Several studies reported that recombinant human OPN is cleaved by MMP-3, MMP-7, and MMP-9 to generate fragments at apparent molecular weights of 40, 32, and 25 kDa [60,61,63]. In a previous study, we demonstrated significant increases in the expression levels of MMP-1, MMP-7, and MMP-9 in vitreous samples from

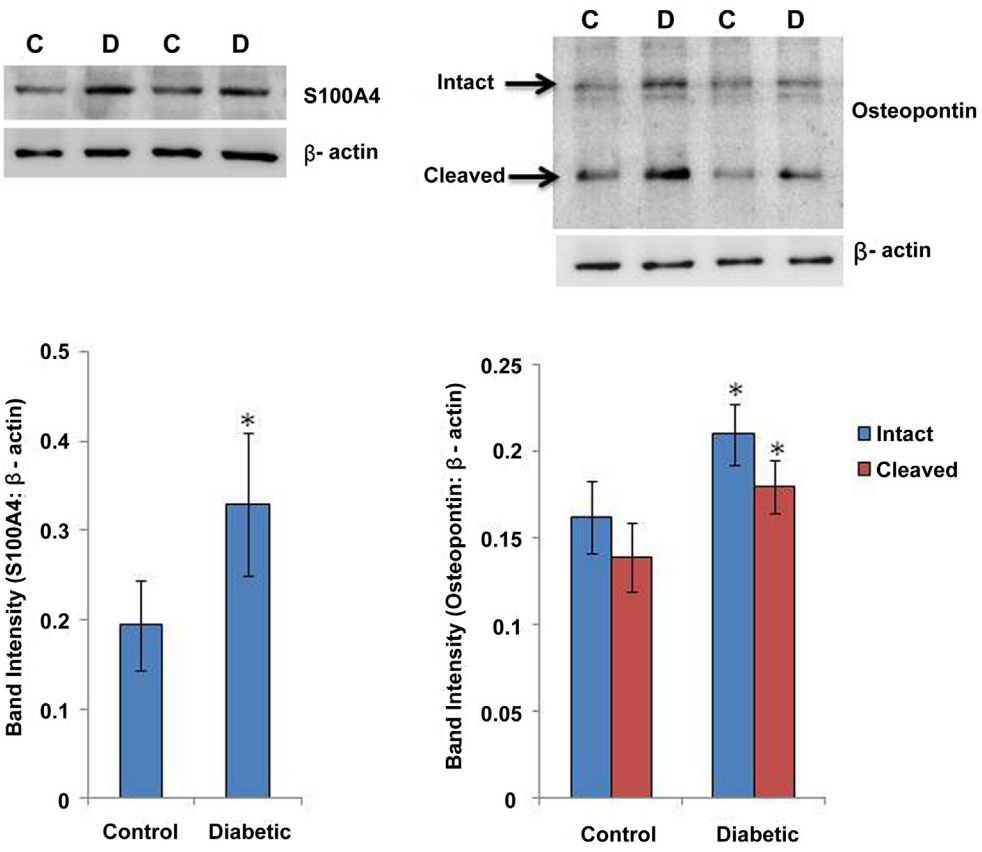

Figure 5. Western blot analysis of S100A4 and OPN in rat retinas. Significant increases in the expressions of S100A4 and both intact and cleaved OPN in the retinas of diabetic rats (**D**) compared to those of the nondiabetic control rats (**C**). Each experiment was repeated 3X with fresh samples (n = 8). *The difference between the two means was statistically significant at the 5% level.

PDR patients [11]. The 40-kDa fragment of OPN significantly promoted more cell adhesion than the full-length protein in several cell lines. Furthermore, this increased cell adhesion was associated with increased cell spreading. In contrast, the 32- and 25-kDa OPN fragments did not promote significant cell adhesion in any cell type tested [64]. These findings suggest that the interaction between OPN and MMPs contributes to the progression of PDR.

In the current study, we found a significant correlation between the vitreous levels of OPN and those of S100A4. This finding is consistent with previous studies in which it was reported that extracellular S100A4 induces NF-κB-dependent expressions and secretions of OPN in osteosarcoma cell lines [45]. These findings suggest that OPN is a downstream molecular mechanism of S100A4 signaling in PDR. Several studies demonstrated that OPN could induce the expression of VEGF in several cell types [35,43]. In agreement with these studies, we demonstrated a significant correlation between the levels of OPN and the levels of VEGF in vitreous fluid. However, in an attempt to corroborate the findings at the cellular level, stimulation with the proinflammatory cytokine TNF-α—but not VEGF—caused an upregulation of OPN in HRMECs. Our findings, however, suggest that inflammatory mediators contribute to the pathogenesis of diabetes-induced retinal vasculopathy. In a previous report, we demonstrated that OPN was expressed by vascular endothelial and stromal cells in PDR fibrovascular epiretinal membranes [60].

In the present study, we showed that the soluble syndecan-1 expression was upregulated in the vitreous fluids of patients with PDR. Previous studies reported that several MMPs, including MMP-2, MMP-3, MMP-7, and MMP-9, induce the shedding of syndecan-1 ectodomains [47]. The shed syndecan-1 accumulates in the sera of patients with some cancer types, whereas high serum levels of syndecan-1 reflect a high tumor burden and predict poor prognosis [46]. High levels of shed syndecan-1 in the tumor microenvironment are associated with elevated angiogenesis and poor prognosis in several types of cancers [65,66]. Elevated levels of shed syndecan-1 and VEGF form matrix-anchored complexes, together, activate the VEGF receptors on adjacent endothelial cells, thereby stimulating tumor angiogenesis [65]. These findings suggest that the MMP/syndecan-1/VEGF axis contributes to PDR progression.

In conclusion, our findings suggest a potential link among S100A4, OPN, soluble syndecan-1, and VEGF in the progression of PDR. A downregulation of S100A4 could be

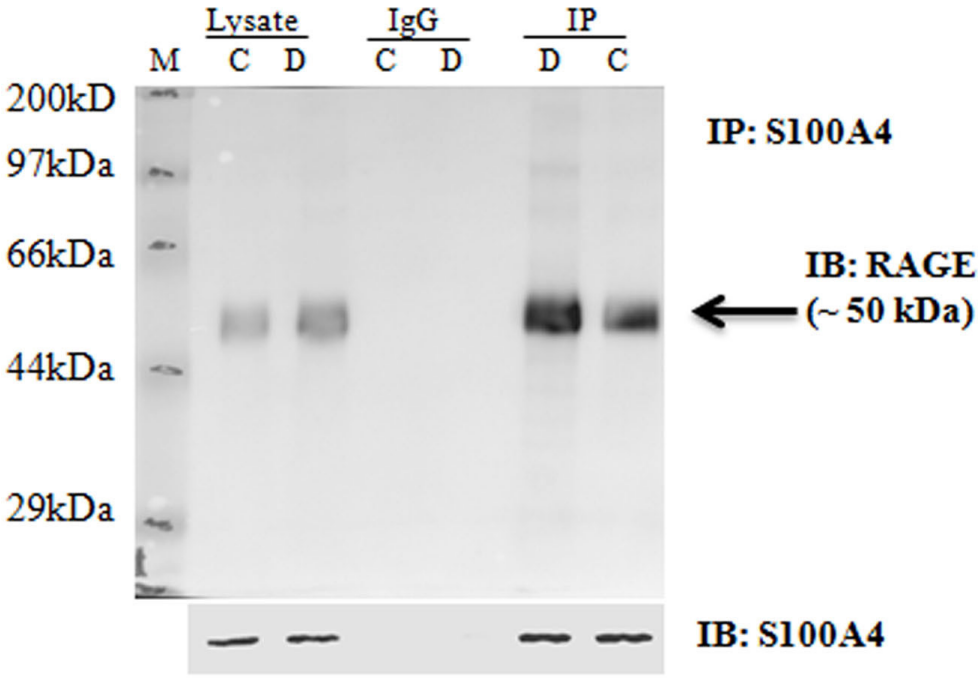

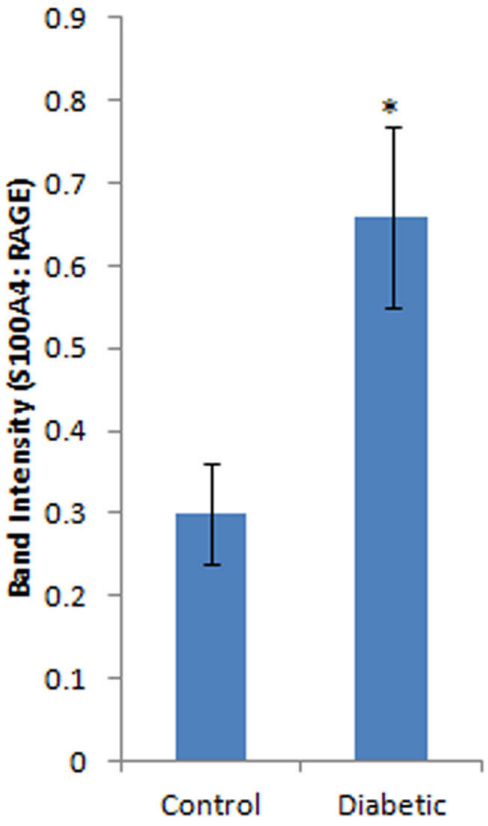

Figure 6. Co-immunoprecipitation of the interaction between S100A4 and the receptor for advanced glycation end products (RAGE) in the retina. Retinal tissue homogenates were immunoprecipitated using an antibody against S100A4 and normal rabbit IgG as a control antibody. The relative abundance of RAGE in the S100A4 immunoprecipitates was determined by western blotting. The level of S100A4 in the immunoprecipitated samples was used as an indicator of loading. Each experiment was repeated 3X with fresh samples (n = 4). *The difference between the two means was statistically significant at the 5% level. IP = immunoprecipitation, IB = immunoblotting, C = control, D = diabetic, IgG = normal rabbit IgG control antibody, Lysate = retinal tissue lysate.

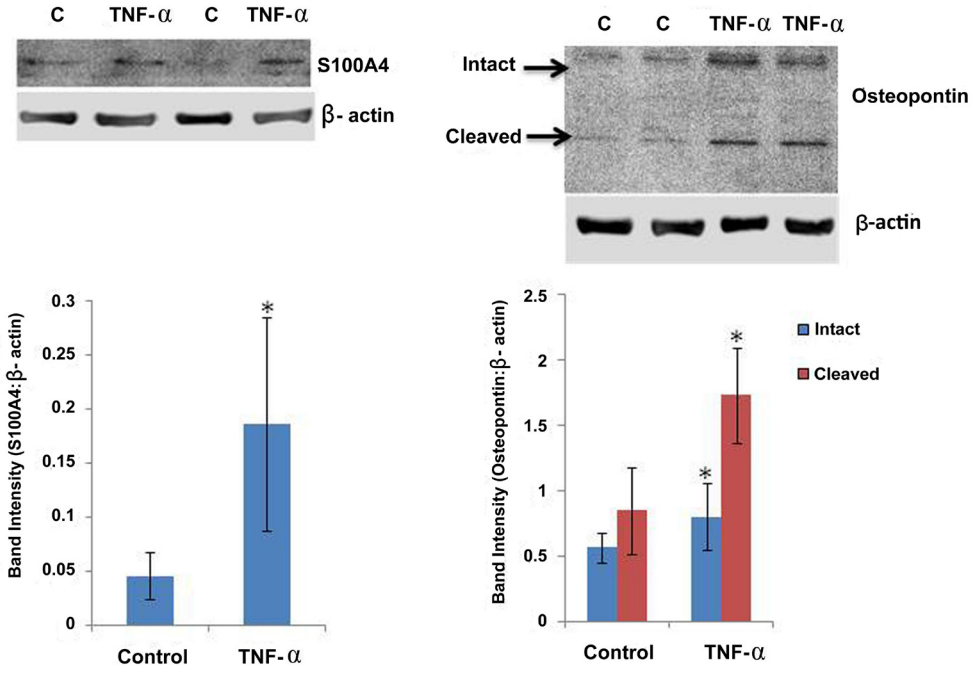

Figure 7. Human retinal microvascular endothelial cells were left untreated (C) or treated with tumor necrosis factor-α (TNF-α) for 6 days. The expression levels of S100A4 and both intact and cleaved OPN were significantly increased in the TNF-α treated samples compared to the controls. Western blot is representative of three different experiments, each performed in triplicate, and bar graphs are representative of all three experiments. *The difference between the two means was statistically significant at the 5% level.

an effective, novel therapeutic approach for the inactivation of its target gene expressions VEGF and OPN, resulting in the inhibition of PDR progression. Regardless of whether such targeting studies fail in the future, the present study clearly demonstrates that S100A4 is a new biomarker in PDR.

ACKNOWLEDGMENTS

The authors thank Mr. Wilfried Versin for technical assistance and Ms. Connie B. Unisa-Marfil for secretarial work. This work was supported by Dr. Nasser Al-Rasheed Research Chair in Ophthalmology (Abu El-Asrar AM) and the Fund for Scientific Research of Flanders (FWO-Vlaanderen, Brussels, Belgium) and the Concerted Research Actions (G.O.A. 2013/014) of the Regional Government of Flanders.

REFERENCES

1. Joussen AM, Poulaki V, Le ML, Koizumi K, Esser C, Janicki H, Schraermeyer U, Kociok N, Fauser S, Kirchhof B, Kern TS. Adamis AP. A central role for inflammation in the pathogenesis of diabetic retinopathy. FASEB J 2004; 18:1450-[PMID: 15231732].
2. Kaji Y, Usui T, Ishida S, Yamashiro K, Moore TC, Moore J, Yamamoto Y, Yamamoto H, Adamis AP. Inhibition of diabetic leukostasis and blood-retinal barrier breakdown with a soluble form of a receptor for advanced glycation end products. Invest Ophthalmol Vis Sci 2007; 48:858-[PMID: 17251488].
3. Kim YW, West XZ, Byzova TV. Inflammation and oxidative stress in angiogenesis and vascular disease. J Mol Med (Berl) 2013; 91:323-8. [PMID: 23430240].
4. Ono M. Molecular links between tumor angiogenesis and inflammation: inflammatory stimuli of macrophages and cancer cells as targets for therapeutic strategy. Cancer Sci 2008; 99:1501-6. [PMID: 18754859].
5. Abu El-Asrar AM, Nawaz MI, Kangave D, Siddiquei MM, Geboes K. Angiogenic and vasculogenic factors in the vitreous from patients with proliferative diabetic retinopathy. J Diabetes Res. 2013; 2013:[PMID: 23671874].
6. Abu El-Asrar AM, Imtiaz Nawaz M, Kangave D, Siddique MM, Geboes K. Osteopontin and other regulators of angiogenesis and fibrogenesis in the vitreous from patients with proliferative vitreoretinal disorders. Mediators Inflamm 2012; 2012:493043-[PMID: 23055574].
7. El-Asrar AM, Nawaz MI, Kangave D, Geboes K, Ola MS, Ahmad S, Al-Shabrawey M. High-mobility group box-1 biomarkers of inflammation in the vitreous from patients with proliferative diabetic retinopathy. Mol Vis 2011; 17:1829-38. [PMID: 21850157].
8. Nawaz MI, Van Raemdonck K, Mohammad G, Kangave D, Van Damme J, Abu El-Asrar AM, Struyf S. Autocrine CCL2, CXCL4, CXCL9 and CXCL10 signal in retinal endothelial cells and are enhanced in diabetic retinopathy. Exp Eye Res 2013; 109:67-76. [PMID: 23352833].
9. Deryugina EI, Quigley JP. Pleiotropic roles of matrix metalloproteinases in tumor angiogenesis: contrasting, overlapping and compensatory functions. Biochim Biophys Acta 2010; 1803:103-20. [PMID: 19800930].

10. Spranger J, Pfeiffer AF. New concepts in pathogenesis and treatment of diabetic retinopathy. Exp Clin Endocrinol Diabetes 2001; 109:Suppl 2S438-50. [PMID: 11460590].

11. Abu El-Asrar AM, Mohammad G, Nawaz MI, Siddique MM, Van den Eynde K, Mousa A, De Hertogh G, Opdenakker G. Relationship between vitreous levels of matrix metalloproteinases and vascular endothelial growth factor in proliferative diabetic retinopathy. PLoS ONE 2013; 8:e85857-[PMID: 24392031].

12. Saleem M, Kweon MH, Johnson JJ, Adhami VM, Elcheva I, Khan N. Bin Hafeez B. Bhat KM, Sarfaraz S. Reagan-Shaw S, Spiegelman VS, Setaluri V, Mukhtar H. S100A4 accelerates tumorigenesis and invasion of human prostate cancer through the transcriptional regulation of matrix metalloproteinase 9. Proc Natl Acad Sci USA 2006; 103:14825-30. [PMID: 16990429].

13. Zhang J, Zhang DL, Jiao XL, Dong Q. S100A4 regulates migration and invasion in hepatocellular carcinoma HepG2 cells via NK-κB-dependent MMP-9 signal. Eur Rev Med Pharmacol Sci 2013; 17:2372-82. [PMID: 24065232].

14. Boye K, Maelandsmo GM. S100A4 and metastasis: a small actor playing many roles. Am J Pathol 2010; 176:528-35. [PMID: 20019188].

15. de Silva Rudland S, Martin L, Roshanlall C, Winstanley J, Leinster S, Platt-Higgins A, Carroll J, West C, Barraclough R, Rudland P. Association of S100A4 and osteopontin with specific prognostic factors and survival of patients with minimally invasive breast cancer. Clin Cancer Res 2006; 12:1192-200. [PMID: 16489073].

16. Tamaki Y, Iwanaga Y, Niizuma S, Kawashima T, Kato T, Inuzuka Y, Horie T, Morooka H, Takase T, Akahashi Y, Kobuke K, Ono K, Shioi T, Sheikh SP, Ambartsumian N, Lukanidin E, Koshimizu T, Miyazaki S, Kimura T. Metastasis-associated protein, S100A4 mediates cardiac fibrosis potentially through the modulation of p53 in cardiac fibroblasts. J Mol Cell Cardiol 2013; 57:72-81. [PMID: 23352991].

17. He J, Xu Y, Koya D, Kanasaki K. Role of the endothelial-to-mesenchymal transition in renal fibrosis of chronic kidney disease. Clin Exp Nephrol 2013; 17:488-97. [PMID: 23430391].

18. Zeisberg EM, Potenta SE, Sugimoto H, Zeisberg M, Kalluri R. Fibroblasts in kidney fibrosis emerge via endothelial-to-mesenchymal transition. J Am Soc Nephrol 2008; 19:2282-7. [PMID: 18987304].

19. Tang RN, Lv LL, Zhang JD, Dai HY, Li Q, Zheng M, Ni J, Ma KL, Liu BC. Effects of angiotensin II receptor blocker on myocardial endothelial-to-mesenchymal transition in diabetic rats. Int J Cardiol 2013; 162:92-9. [PMID: 21704391].

20. Widyantoro B, Emoto N, Nakayama K, Anggrahini DW, Adiarto S, Iwasa N, Yagi K, Miyagawa K, Rikitake Y, Suzuki T, Kisanuki YY, Yanagisawa M, Hirata K. Endothelial cell-derived endothelin-1 promotes cardiac fibrosis in diabetic hearts through stimulation of endothelial-to-mesenchymal transition. Circulation 2010; 121:2407-18. [PMID: 20497976].

21. Österreicher CH, Penz-Österreicher M, Grivennikov SI, Guma M, Koltsova EK, Datz C, Sasik R, Hardiman G, Karin M, Brenner DA. Fibroblast-specific protein 1 identified an inflammatory subpopulation of macrophages in the liver. Proc Natl Acad Sci USA 2011; 108:308-13. [PMID: 21173249].

22. Senolt L, Grigorian M, Lukanidin E, Simmen B, Michel BA, Pavelka K, Gay RE, Gay S, Neidhart M. S100A4 is expressed at site of invasion in rheumatoid arthritis synovium and modulates production of matrix metalloproteinases. Ann Rheum Dis 2006; 65:1645-8. [PMID: 17105852].

23. Klingelhöfer J, Senolt L, Baslund B, Nielsen GH, Skibshøj I, Pavelka K, Neidhart M, Gay S, Ambartsumian N, Hansen BS, Petersen J, Lukanidin E, Grigorian M. Up-regulation of metastasis-promoting S100A4 (Mts-1) in rheumatoid arthritis: putative involvement in the pathogenesis of rheumatoid arthritis. Arthritis Rheum 2007; 56:779-789-[PMID: 17328050].

24. Oslejsková L, Grigorian M, Gay S, Neidhart M, Senolt L. The metastasis associated protein S100A4: a potential novel link to inflammation and consequent aggressive behavior of rheumatoid arthritis synovial fibroblasts. Ann Rheum Dis 2008; 67:1499-504. [PMID: 18056757].

25. Schneider M, Hansen J, Sheikh SP. S100A4: a common mediator of epithelial-mesenchymal transition, fibrosis and regeneration in diseases? J Mol Med (Berl) 2008; 86:507-22. [PMID: 18322670].

26. Helfman DM, Kim EJ, Lukanidin E, Grigorian M. The metastasis associated protein S100A4: role in tumour progression and metastasis. Br J Cancer 2005; 92:1955-8. [PMID: 15900299].

27. Jia W, Gao XJ, Zhang ZD, Yang ZX, Zhang G. S100A4 silencing suppresses proliferation, angiogenesis and invasion of thyroid cancer cells through downregulation of MMP-9 and VEGF. Eur Rev Med Pharmacol Sci 2013; 17:1495-508. [PMID: 23771538].

28. O'Connell JT, Sugimoto H, Cooke VG, MacDonald BA, Mehta AI, LeBleu VS, Dewar R, Rocha RM, Brentani RR, Resnick MB, Neilson EG, Zeisberg M, Kalluri R. VEGF-A and Tenascin-C produced by S100A4+ stromal cells are important for metastatic colonization. Proc Natl Acad Sci USA 2011; 108:16002-7. [PMID: 21911392].

29. Kelly DJ, Chanty A, Gow RM, Zhang Y, Gilbert RE. Protein kinase CB inhibition attenuates osteopontin expression, macrophage recruitment, and tubulointerstitial injury in advanced experimental diabetic nephropathy. J Am Soc Nephrol 2005; 16:1654-60. [PMID: 15843473].

30. Naldini A, Leali D, Pucci A, Morena E, Carraro F, Nico B, Ribatti D, Presta M. Cutting edge: IL-1 β mediates the proangiogenic activity of osteopontin-activated human monocytes. J Immunol 2006; 177:4267-70. [PMID: 16982859].

31. Kohan M, Breuer R, Berkman N. Osteopontin induces airway remodeling and lung fibroblast activation in a murine model of asthma. Am J Respir Cell Mol Biol 2009; 41:290-6. [PMID: 19151319].

32. Pardo A, Gibson K, Cisneros J, Richards TJ, Yang Y, Becerril C, Yousem S, Herrera I, Ruiz V, Selman M, Kaminski N. Up-regulation and profibrotic role of osteopontin in human idiopathic pulmonary fibrosis. PLoS Med 2005; 2:e251-[PMID: 16128620].

33. Lenga Y, Koh A, Perera AS, McCulloch CA, Sodek J, Zohar R. Osteopontin expression is required for myofibroblast differentiation. Circ Res 2008; 102:319-27. [PMID: 18079410].

34. Sabo-Attwood T, Ramos-Nino ME, Eugenia-Ariza M, MacPherson MB, Butnor KJ, Vacek PC, McGee SP, Clark JC, Steele C, Mossman BT. Osteopontin modulates inflammation, mucin production, and gene expression signatures after inhalation of asbestos in a murine model of fibrosis. Am J Pathol 2011; 178:1975-85. [PMID: 21514415].

35. Dai J, Peng L, Fan K, Wang H, Wei R, Ji G, Cai J, Lu B, Li B, Zhang D, Kang Y, Tan M, Qian W, Guo Y. Osteopontin induces angiogenesis through activation of PI3K/AKT and ERK1/2 in endothelial cells. Oncogene 2009; 28:3412-22. [PMID: 19597469].

36. Cui R, Takahashi F, Ohashi R, Gu T, Yoshioka M, Nishio K, Ohe Y, Tominaga S, Takagi Y, Sasaki S, Fukuchi Y, Takahashi K. Abrogation of the interaction between osteopontin and $\alpha_v\beta_3$ integrin reduces tumor growth of human lung cancer cells in mice. Lung Cancer 2007; 57:302-10. [PMID: 17482311].

37. Du XL, Jiang T, Sheng XG, Gao R, Li QS. Inhibition of osteopontin suppresses *in vitro* and *in vivo* angiogenesis in endometrial cancer. Gynecol Oncol 2009; 115:371-6. [PMID: 19783287].

38. Wang Y, Yan W, Lu X, Qian C, Zhang J, Li P, Shi L, Zhao P, Fu Z, Pu P, Kang C, Jiang T, Liu N, You Y. Overexpression of osteopontin induces angiogenesis of endothelial progenitor cells via the αvβ3/PI3K/AKT/eNOS/NO signaling pathway in glioma cells. Eur J Cell Biol 2011; 90:642-8. [PMID: 21616556].

39. Denhardt DT, Noda M, O'Regan AW, Pavlin D, Berman JS. Osteopontin as a means to cope with environmental insults: regulation of inflammation, tissue remodeling, and cell survival. J Clin Invest 2001; 107:1055-61. [PMID: 11342566].

40. Huang Q, Sheibani N. High glucose promotes retinal endothelial migration through activation of Src, PI3K/Akt1/eNOS, and ERKs. Am J Physiol Cell Physiol 2008; 295:C1647-57. [PMID: 18945941].

41. Takemoto M, Yokotc K, Nishimura M, Shigematsu T, Hasegawa T, Kon S, Uede T, Matsumoto T, Saito Y, Mori S. Enhanced expression of osteopontin in human diabetic artery and analysis of its functional role in accelerated atherogenesis. Arterioscler Thromb Vasc Biol 2000; 20:624-8. [PMID: 10712383].

42. Junaid A, Amara FM. Osteopontin: correlation with interstitial fibrosis in human diabetic kidney and PI3-kinase-mediated enhancement of expression by glucose in human proximal tubular epithelial cells. Histopathology 2004; 44:136-46. [PMID: 14764057].

43. Chakraborty G, Jain S, Kundu GC. Osteopontin promotes vascular endothelial growth factor-dependent breast tumor growth and angiogenesis via autocrine and paracrine mechanisms. Cancer Res 2008; 68:152-61. [PMID: 18172307].

44. Berge G, Pettersen S, Grotterød I, Bettum IJ, Boye K, Mælandsmo GM. Osteopontin—an important downstream effector of S100A4-mediated invasion and metastasis. Int J Cancer 2011; 129:780-90. [PMID: 20957651].

45. Teng YH, Aquino RS, Park PW. Molecular functions of syndecan-1 in disease. Matrix Biol 2012; 31:3-16. [PMID: 22033227].

46. Manon-Jensen T, Multhaupt HAB, Couchman JR. Mapping of matrix metalloproteinase cleavage sites on syndecan-1 and syndecan-4 ectodomains. FEBS J 2013; 280:2320-31. [PMID: 23384311].

47. Aiello LP, Avery RL, Arrig PG, Keyt BA, Jampel HD, Shah ST, Pasquale LR, Thieme H, Iwamoto MA, Park JE, Nguyen HV, Aiello LM, Ferrara N, King GL. Vascular endothelial growth factor in ocular fluid in patients with diabetic retinopathy and other retinal disorders. N Engl J Med 1994; 331:1480-7. [PMID: 7526212].

48. Bishop PN. Structural macromolecules and supramolecular organization of the vitreous gel. Prog Retin Eye Res 2000; 19:323-44. [PMID: 10749380].

49. Sebag J. Anomalous posterior vitreous detachment: a unifying concept in vitreo-retinal disease. Graefes Arch Clin Exp Ophthalmol 2004; 242:690-8. [PMID: 15309558].

50. van Deemter M, Pas HH, Kuijer R, van der Worp RJ, Hooymans JM, Los LI. Enzymatic breakdown of type II collagen in the human vitreous. Invest Ophthalmol Vis Sci 2009; 50:4552-60. [PMID: 19420340].

51. Abu El-Asrar AM, Missotten L, Geboes K. Expression of advanced glycation end products and related molecules in diabetic fibrovascular epiretinal membranes. Clin Experiment Ophthalmol 2010; 38:57-64. [PMID: 20447102].

52. Le Hir M, Hegyi I, Cueni-Loffing D, Loffing J, Kaissling B. Characterization of renal interstitial fibroblast-specific protein 1/S100A4-positive cells in healthy and inflamed rodent kidneys. Histochem Cell Biol 2005; 123:335-46. [PMID: 15856273].

53. Ambartsumian N, Klingelhöfer J, Grigorian M, Christensen C, Kriajevska M, Tulchinsky E, Georgiev G, Berezin V, Bock E, Rygaard J, Cao R, Cao Y, Lukanidin E. The metastasis-associated Mts1 (S100A4) protein could act as an angiogenic factor. Oncogene 2001; 20:4685-95. [PMID: 11498791].

54. Hernández JL, Padilla L, Dakhel S, Coll T, Hervas R, Adan J, Masa M, Mitjans F, Martinez JM, Coma S, Rodríguez L, Noé V, Ciudad CJ, Blasco F, Messeguer R. Therapeutic targeting of tumor growth and angiogenesis with a novel anti-S100A4 monoclonal antibody. PLoS ONE 2013; 8:e72480-[PMID: 24023743].

55. Ochiya T, Takenaga K, Endo H. Silencing of S100A4, a metastasis-associated protein, in endothelial cells inhibits

tumor angiogenesis and growth. Angiogenesis 2014; 17:17-26. [PMID: 23929008].

56. Yang H, Zhao K, Yu Q, Wang X, Song Y, Li R. Evaluation of plasma and tissue S100A4 protein and mRNA levels as potential markers of metastasis and prognosis in clear cell renal cell carcinoma. J Int Med Res 2012; 40:475-85. [PMID: 22613408].

57. Ai KX, Lu LY, Huang XY, Chen W, Zhang HZ. Prognostic significance of S100A4 and vascular endothelial growth factor expression in pancreatic cancer. World J Gastroenterol 2008; 14:1931-5. [PMID: 18350635].

58. Dahlmann M, Okhrimenko A, Marcinkowski P, Osterland M, Herrmann P, Smith J, Heizmann CW, Schlag PM, Stein U. RAGE mediates S100 A4-induced cell motility via MAPK/ERK and hypoxia signaling and is a prognostic biomarker for human colorectal cancer metastasis. Oncotarget 2014; 5:3220-33. [PMID: 24952599].

59. Mohammad G, Siddique MM, Othman A, Al-Shabrawey M, Abu El-Asrar AM. High-mobility group box-1 protein activates inflammatory signaling pathway components and disrupts retinal vascular-barrier in diabetic retina. Exp Eye Res 2013; 107:101-9. [PMID: 23261684].

60. El-Asrar AM, Missotten L, Geboes K. Expression of high-mobility groups box-1/receptor for advanced glycation end products/osteopontin/early growth response-1 pathway in proliferative vitreoretinal epiretinal membranes. Mol Vis 2011; 17:508-18. [PMID: 21365018].

61. Agnihotri R, Crawford HC, Haro H, Matrisian LM, Havrda MC, Liaw L. Osteopontin, a novel substrate for matrix metalloproteinase-3 (Stromelysin-1) and matrix metalloproteinase-7 (Matrilysin). J Biol Chem 2001; 276:28261-7. [PMID: 11375993].

62. Takafuji V, Forgues M, Unsworth E, Goldsmith P, Wang XW. An osteopontin fragment is essential for tumor cell invasion in hepatocellular carcinoma. Oncogene 2007; 26:6361-71. [PMID: 17452979].

63. Tan TK, Zheng G, Hsu T, Lee SR. zhang J, Zhao Y, Tian X, Wang Y, Wang YM, Cao Q, Wang Y, Lee VWS, Wang C, Zheng D, Alexander SI, Thompson E, Harris DCH. Matrix metalloproteinase-9 of tubular and macrophage origin contributes to the pathogenesis of renal fibrosis via macrophage recruitment through osteopontin cleavage. Lab Invest 2013; 93:434-49. [PMID: 23358111].

64. Gao YA, Agnihotri R, Vary CPH, Liaw L. Expression and characterization of recombinant osteopontin peptides representing matrix metalloproteinase proteolytic fragments. Matrix Biol 2004; 23:457-66. [PMID: 15579312].

65. Purushothaman A, Uyama T, Kobayashi F, Yamada S, Sugahara K, Rapraeger AC, Sanderson RD. Heparanase-enhanced shedding of syndecan-1 by myeloma cells promotes endothelial invasion and angiogenesis. Blood 2010; 115:2449-57. [PMID: 20097882].

66. Yang Y, MacLeod V, Miao H, Theus A, Zhan F, Shaughnessy JD Jr, Sawyer J, Li J, Zcharia E, Vlodavsly I, Sanderson RD. Haparanase enhances syndecan-1 shedding. A novel mechanism for stimulation of tumor growth and metastasis. J Biol Chem 2007; 282:13326-33. [PMID: 17347152].

Articles are provided courtesy of Emory University and the Zhongshan Ophthalmic Center, Sun Yat-sen University, P.R. China. The print version of this article was created on 10 September 2014. This reflects all typographical corrections and errata to the article through that date. Details of any changes may be found in the online version of the article.